OXFORD JOURNAL
OF STUDENT
SCHOLARSHIP

$FeCl_3$ Crosslinking on FeOOH-Immobilized Sodium Alginate Hydrogels for Improved Phosphate Adsorption

Andrew Ni
andrewsyni@gmail.com

ABSTRACT

Phosphate pollution is a significant global issue, causing eutrophication and contaminating wastewater. Iron hydroxide-based adsorbents, such as FeOOH immobilized alginate hydrogels, are commonly investigated for their use in phosphate removal and have potential for further modification. However, current modification methods to improve adsorption performance often do not maximize efficiency and scalability. The present study aimed to evaluate the effect of $FeCl_3$ crosslinking on FeOOH immobilized alginate hydrogels to improve phosphate adsorption capacity and kinetics by introducing additional Fe(III) adsorption sites. It was hypothesized that if FeOOH immobilized alginate hydrogels were crosslinked with $FeCl_3$, the adsorption capacity and kinetics of the hydrogel for phosphate adsorption would improve. FeOOH and alginate hydrogels were synthesized using standardized methods. Adsorption studies with an orbital shaker and a molybdenum colorimetric method were performed. The ferric chloride crosslinked hydrogel (FeCl-Alg) increased adsorption capacity significantly across multiple concentrations and time intervals ($p < 0.05$), increasing it from 321.79 mg/g to 376.14 mg/g at the highest tested concentration (32 ppm). Isotherm and kinetic modeling indicated a more complex adsorption process following $FeCl_3$ treatment, consistent with changes in adsorption behavior of the hydrogel. The improved adsorption performance is consistent with greater Fe(III) adsorption sites increasing phosphate adsorption and accessibility. This study indicates that $FeCl_3$ crosslinking provides an efficient and scalable strategy for potentially improving other adsorbents in the future.

INTRODUCTION

Modernization and industrial activities have led to the excessive release of phosphate into the environment, causing eutrophication and harmful algal blooms in aquatic systems, which have cost the U.S. alone more than $2.2 billion annually (1). Intense phosphate pollution also kills aquatic life and threatens drinking water quality. Phosphates are also limited natural mineral resources that need to be recovered. Phosphate depletion and pollution have thus become global issues for food and ecological security (2). Amorphous metal hydroxides are the most used technology for the removal of phosphates in wastewater treatment through adsorption and precipitation (2). Among these hydroxides, amorphous iron oxide, or FeOOH, often exhibits high phosphate adsorption capacity due to its large number of binding sites (4, 5, 6) and is thus one of the most investigated among these hydroxides in wastewater treatment

(12). Iron hydroxides, however, face issues such as inefficiencies, lack of reusability, and difficult handling (7). To solve these issues, prior literature has immobilized FeOOH onto polymers such as clay (8), melamine sponge (9), and composites (3), making the FeOOH more reusable, applicable, and efficient. Among these, alginate hydrogels have seen the greatest success in serving as a polymer base for FeOOH, as noted by Yang et al. (11), where FeOOH immobilized alginate hydrogels (Ca-Alg) had significantly improved phosphate adsorption capacity (Q_e = 24.2 mg/g), a step up from raw FeOOH by 1.9 times, while remaining reusable over multiple cycles. However, despite these improvements, the adsorption capacity of FeOOH-immobilized hydrogels remains limited by the finite number and accessibility of adsorption sites within the matrix (6, 10, 11). Consequently, further modification strategies that increase available adsorption sites within the hydrogel without compromising other factors remain an important area of research, as previous approaches in iron-based adsorbents have often been inefficient and non-scalable (13). Thus, developing a simple, scalable method to enhance the adsorption performance of FeOOH-immobilized alginate hydrogels could improve phosphate removal efficiency while maintaining the practical advantages of these materials.

Ferric ions (Fe^{3+}) are well known to interact strongly with both alginate polymers and phosphate. Crosslinking with Fe^{3+} produces strong ionic crosslinks and introduces adsorption sites having high affinity to phosphate while remaining environmentally friendly and scalable (4, 5, 6). These structural and chemical effects together have led to the success of Fe^{3+} crosslinked hydrogels in many adsorption studies (14). Although previous studies have primarily investigated $FeCl_3$ crosslinking to improve the adsorption capabilities of alginate hydrogels, its influence on the recent FeOOH immobilized alginate hydrogels is unknown (10, 11). Understanding how ferric crosslinking could improve upon and modify FeOOH immobilized hydrogels could provide a practical strategy for enhancing phosphate adsorption efficiency in wastewater treatment.

This study investigated whether post-synthesis $FeCl_3$ treatment of FeOOH immobilized alginate hydrogels influences phosphate adsorption by creating additional Fe(III)-based adsorption sites. This study hypothesized that if FeOOH immobilized alginate hydrogels were crosslinked with $FeCl_3$, the adsorption capacity and kinetics of the hydrogel for phosphate adsorption would improve.

MATERIALS AND METHODS

Hydrogel Formation

FeOOH nanoparticles were first prepared using the standard Cornell and Schwertmann method (16). First, a 1M solution of NaOH was added dropwise into a 0.5M solution of $FeCl_3$ (Carolina Chemicals 86-2480) under a magnetic stirrer, with pH kept below 7.5 to produce amorphous FeOOH. After this, the fresh precipitates were washed and let sit for two hours. Next, two separate sodium alginate solutions were prepared by slowly dissolving 10 g sodium alginate (ChemCenter 9005-38-3) in 500 mL distilled water (2% w/v) and labeled as FeCl-Alg and Ca-Alg. Fifty grams of FeOOH were weighed out with a scale and stirred into each alginate solution. Hydrogels were formed using the extrusion dropping method by slowly pipetting both solutions dropwise into 0.27 M $CaCl_2$ (Sturelehub SEHACC001) crosslinking baths and

then decanting and washing with distilled water until pH = 7 (10, 11). The Ca-Alg group was left unmodified, while the FeCl-Alg group was immersed in a 0.1 M $FeCl_3$ (Carolina Chemicals 86-2480) solution for 10 minutes and then decanted and washed.

Adsorption Experiments

A serial dilution was done with varying concentrations of KH_2PO_4 (Loudwolf 7778-77-0) to obtain bottles of 2, 4, 8, 16, and 32 mg/L phosphate solutions. Higher phosphate concentrations were tested in order to assess a wider concentration range. Furthermore, limitations in methodology do not allow accurate monitoring of meaningful differences in lower concentrations. A standard molybdenum-based colorimetric assay (11) and a smartphone RGB color identification app called “Color Identification” in consistent lighting were used to form a calibration curve (Figure 1), plotting B values against known concentrations to determine unknown phosphate concentrations in the adsorption experiments. Each concentration was measured over 10 trials. The colorimetric assay was done using a phosphate test kit (API), with six drops of 40% sulfuric acid (Mars Fishcare North America 1595-023) and molybdenum blue indicator (Mars Fishcare North America 1557-05) added into a test tube of 5 ml phosphate solution. The calibration curve was determined over a phosphate concentration range of 0-8 mg/L. To ensure all measurements fell within this calibrated range, samples with phosphate concentrations exceeding 8 mg/L were diluted prior to analysis. Specifically, samples originating from 16 mg/L and 32 mg/L phosphate solutions were diluted by factors of 2 and 4, respectively, before colorimetric measurement. The equilibrium phosphate concentrations obtained from the calibration curve were subsequently multiplied by the corresponding dilution factor to determine the concentration in the undiluted sample.

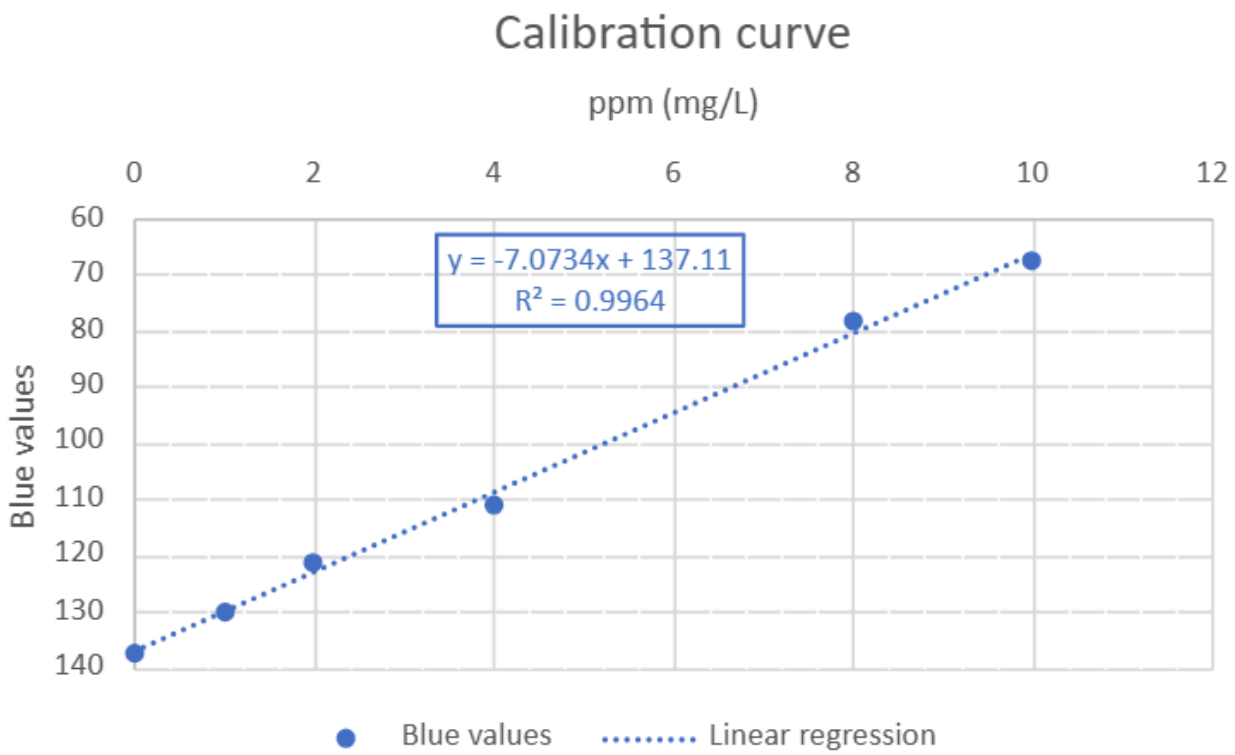


Figure 1. This scatterplot shows varying phosphate concentrations (0-10 mg/L) with respect to blue RGB values. Blue values were derived from a molybdenum colorimetric method and smartphone color identifier. Regression line (y=-7.0734x+137.11), R^2=0.9857, n=10.

Batch adsorption studies were conducted to assess the adsorption capacity and kinetics of the adsorbent. All adsorption experiments were conducted by shaking ten 100 mL beakers containing 3.3 mg of wet hydrogel and 50 mL of a singular phosphate solution using an orbital shaker at 100 rpm for eight hours, with the resulting phosphate solution being measured with the colorimetric assay and calibration curve. Adsorption experiments also included blanks with no adsorbent to measure the accuracy of the calibration curve method. For the adsorption capacity test, adsorption experiments were conducted at each individual concentration level ten times for both hydrogel groups. For adsorption kinetics tests, adsorption experiments were done at a constant 32 mg/L phosphate concentration with ten trials for both hydrogel groups, and samples were collected using a syringe at set time intervals (5, 15, 30, 60, 180, and 480 min) into different containers and then measured. Iron leaching tests were done by putting five grams of hydrogel into ten 100 mL beakers of distilled water for both groups and taking measurements with a pH meter after waiting 48 hours.

Data Analysis

The equilibrium phosphate concentrations were used to determine the maximum adsorption capacity and removal efficiency of the hydrogels. RGB value data was plugged into the equations and adsorption

models through Microsoft Excel, and adsorption parameters were derived through trendline regressions. T-tests were then conducted with the adsorption data in Microsoft Excel, and the parameters were derived. The adsorption mass balance equation [Eqn 1] was used to determine the capacity of the adsorbent to bind phosphate and derive adsorption model values.

$$Q_{e,t} = \frac{(C_o - C_{e,t})}{m} \times v \qquad \text{[Equation 1]}$$

Here, Q_e and Q_t represent the adsorption capacity and capacity at time t (mg g^{-1}), C_o, C_e, and C_t are the initial concentrations, final concentrations, and concentration at time t (mg L^{-1}), v is the volume of the solution (mL), and m is the total mass of the hydrogels (g). The following equation [Eqn 2] was used to determine percent phosphate removal efficiency.

The adsorption isotherm measures the equilibrium relationship between the adsorbate on the adsorbent surface and the concentration of the adsorbate in the surrounding phase at a constant temperature. Isotherm models give essential insights into the mechanisms of the adsorption process (17).

$$R(\%) = \frac{(C_o - C_{e,t})}{m} \times 100 \qquad \text{[Equation 2]}$$

The linear Freundlich isotherm model [Eqn 3] indicates complex, multilayered adsorption and heterogeneous adsorption sites. The linear Langmuir isotherm model [Eqn 4] assumes a homogenous adsorption process and localized chemisorption on the surface (18).

$$ln(Q_e) = ln(K_F) + \frac{1}{n} ln(C_e) \qquad \text{[Equation 3]}$$

$$\frac{C_e}{Q_e} = \frac{C_e}{Q_{max}} + \frac{1}{Q_{max} \times K_L} \qquad \text{[Equation 4]}$$

Qe represents the amount of phosphate adsorbed per unit mass of the adsorbent (mg g^{-1}), KF is the Freundlich constant, n is the Freundlich exponent, C_e is the equilibrium adsorbate concentration, Q_{max} is the maximum adsorbate amount for monolayer adsorption (mg g^{-1}), and KL is the Langmuir constant.

Adsorption kinetic models describe the rate at which the adsorbate binds to the adsorbent during the adsorption process (19). The pseudo-first-order model [Eqn 5] assumes that the rate of occupation of adsorption sites is proportional to the number of unoccupied sites, describing a simpler physisorption process. The pseudo-second-order model [Eqn 6] assumes electrons being shared between the adsorbate and adsorbent, indicating chemisorption. The intraparticle diffusion model [Eqn 7] determines if the diffusion within the pores of the adsorbent is the rate limiting step (18).

$$log(Q_e - Q_t) = log(Q_e) - K_1 t \qquad \text{[Equation 5]}$$

$$\frac{t}{Q_t} = \frac{1}{K_2 (Q_e)^2} + \frac{t}{Q_e} \qquad \text{[Equation 6]}$$

$$Q_t = K_{id} t^{0.5} + C \qquad \text{[Equation 7]}$$

Here, t represents the time (min), Qt represents the adsorbate adsorbed at time t (mg g^{-1}), K_1 is the pseudo-first-order rate constant (min^{-1}), K_2 is the pseudo-second-order rate constant (g mg^{-1} min^{-1}), K_{id} is the intraparticle diffusion rate constant (mg g^{-1} $min^{-1/2}$), and C is the boundary layer thickness.

RESULTS

Isotherms and Kinetic Adsorption Models

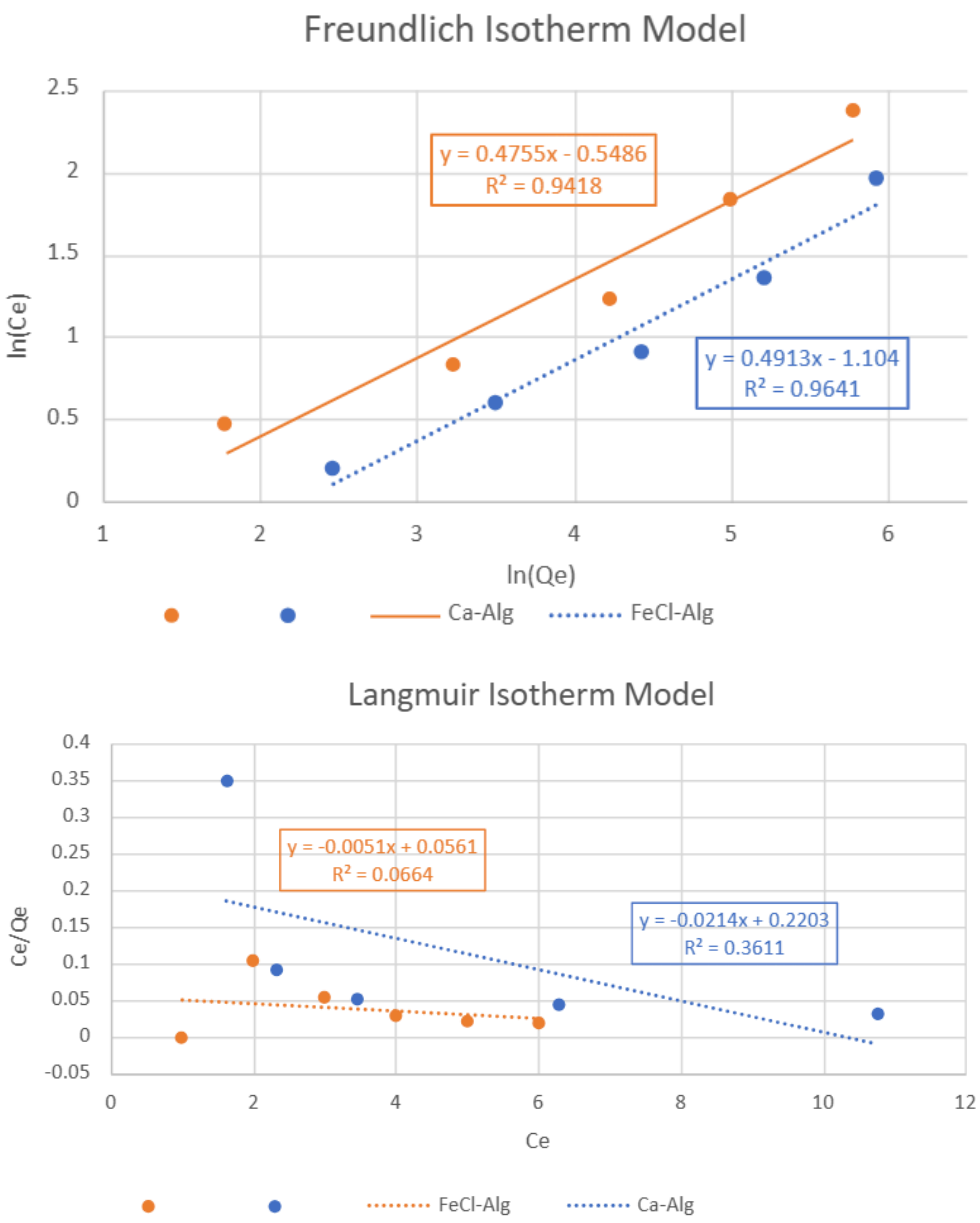


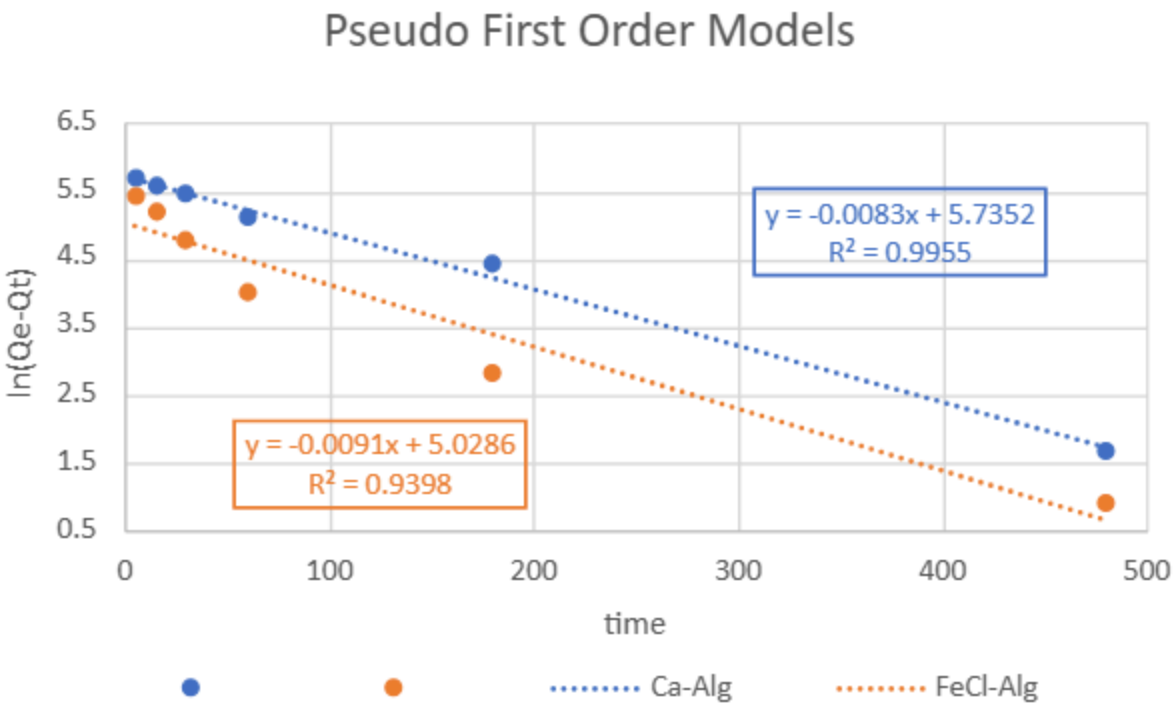
Figure 2. These scatterplots model the adsorption data derived from the mass balance equation. The Langmuir isotherm plots C_e/Q_e over C_e, while the Freundlich isotherm plots ln Q_e over ln C_e. Freundlich Isotherm Regression: Ca-Alg (y=0.4755x-0.5486, R^2=0.9418), FeCl-Alg (y=0.4913x-1.104, R^2=0.9641).

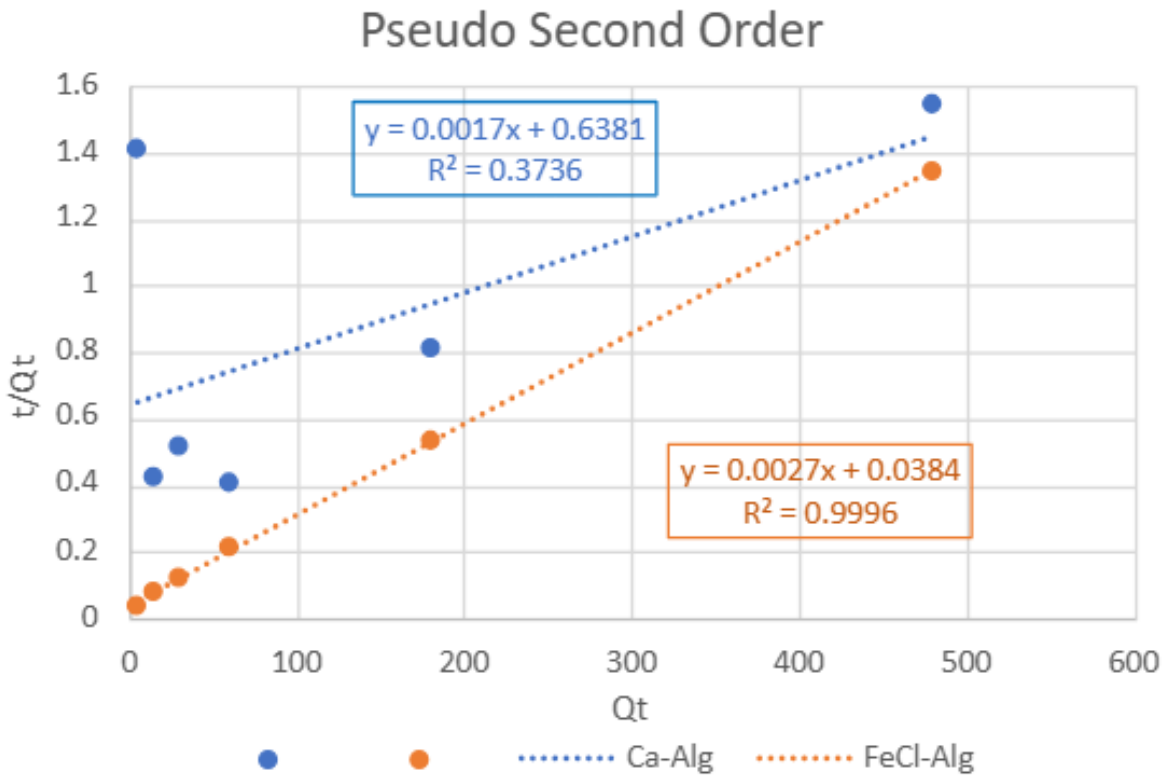
Langmuir Isotherm Regression: Ca-Alg (y=-0.0214x+0.2203, R^2=0.3611), FeCl-Alg (y=-0.0051x+0.0561, R^2=0.0664). n=10.

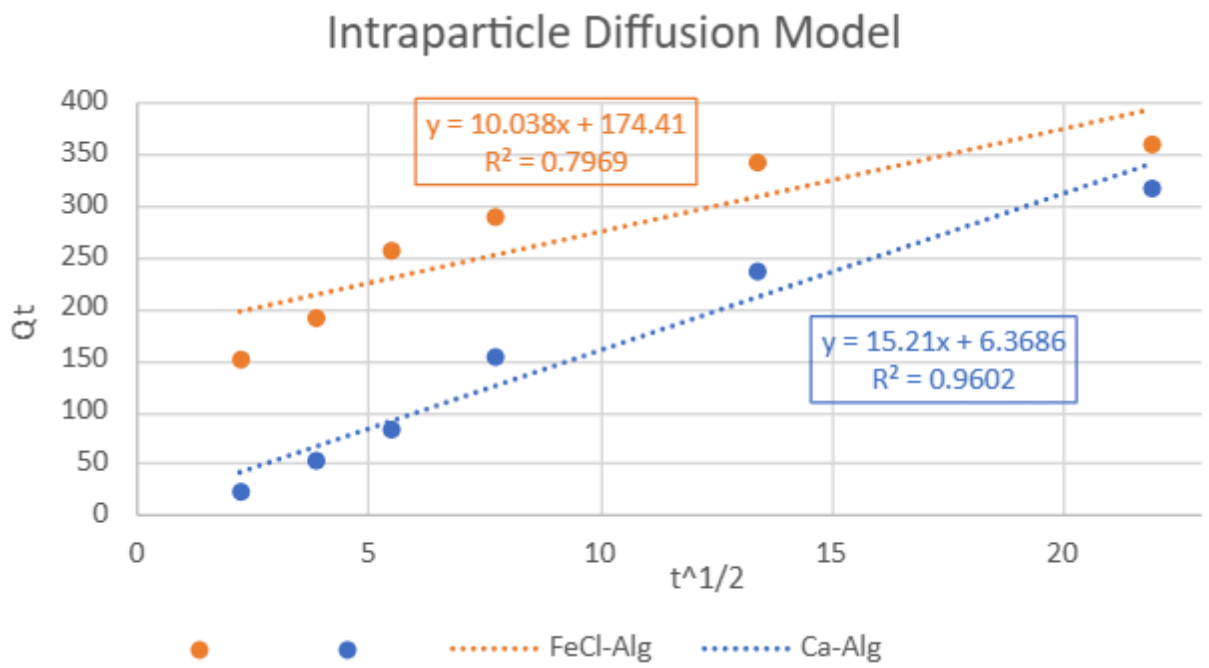
Adsorption Model	Parameters	Ca-Alg	FeCl-Alg
	K_F	0.332	0.578
Freundlich Isotherm	1/n	0.491	0.476
	R^2	0.964	0.942
	K_1	$8.3*10^{-3}$	$9.1*10^{-3}$
Pseudo First-Order	R^2	0.9955	0.9398
	K_{id}	15.20	10.04
	Q_e	588.24	370.37
Pseudo Second-Order	R^2	0.374	0.999
	K_2	$4.5*10^{-6}$	$1.9*10^{-4}$
Intraparticle Diffusion	C	6.37	174.4
	R^2	0.96	0.797

Table 1. The table shows the Freundlich isotherm, pseudo-first-order kinetic, pseudo-second-order kinetic, and intraparticle diffusion model parameters**.** Values were derived from fitting experimental adsorption data onto a line of best fit and calculating parameters using the equation. Corresponding R^2 values are included in each model. n=10.

Both hydrogel groups were found to strongly fit the Freundlich isotherm model (R^2 = 0.94, 0.96), indicating heterogeneous adsorption binding sites (Figure 2). Further, FeCl-Alg exhibited greater adsorption affinity for phosphate compared to Ca-Alg (K_F = 0.578 mg/g vs. 0.332 mg/g), consistent with its additional adsorption sites (Table 1). Note that data calculated for the pseudo-second-order model for Ca-Alg as well as the Langmuir isotherm cannot be used due to poor fits.


Pseudo First Order Models
6.5
5.5
4.5
3.5
2.5
1.5
0.5
ln(Qe-Qt)
0
100
200
300
400
500
time
y = -0.0083x + 5.7352
R² = 0.9955
y = -0.0091x + 5.0286
R² = 0.9398
Ca-Alg
FeCl-Alg


Pseudo Second Order
1.6
1.4
1.2
1
0.8
0.6
0.4
0.2
0
t/Qt
0
100
200
300
400
500
600
Qt
y = 0.0017x + 0.6381
R² = 0.3736
y = 0.0027x + 0.0384
R² = 0.9996
Ca-Alg
FeCl-Alg



Pseudo-First Order, Pseudo-Second Order, and Intraparticle Diffusion Kinetic Adsorption Models

Figure 3. The scatterplots model the adsorption data derived from the mass balance equation. The pseudo-first-order kinetic model plots $\ln(Q_e - Q_t)$ over t, the pseudo-second-order kinetic model plots t/Q_t over t, and the intraparticle diffusion model plots Q_t over $t^{1/2}$. Pseudo-First Order Regression: Ca-Alg (y=-0.0083x+5.7352, R^2=0.9955), FeCl-Alg (y=-0.0091x+5.0286, R^2=0.9398). Pseudo-Second Order Regression: Ca-Alg (y=0.0017x+0.6381, R^2=0.3736), FeCl-Alg (y=0.0027x+0.0384, R^2=0.9996). Intraparticle Diffusion Regression: Ca-Alg (y=15.21x+6.3686, R^2=0.9602), FeCl-Alg (y=10.038x+174.41, R^2=0.7969). n=10.

Both FeCl-Alg and Ca-Alg were found to follow the pseudo-first-order kinetic model (R^2 = 0.94, 0.99), indicating that physisorption was present in the adsorption behavior of both hydrogels. However, FeCl-Alg was an even stronger fit for the pseudo-second-order kinetic model (R^2 = 0.99), suggesting that FeCl-Alg involved additional adsorption processes on top of physisorption, likely due to the $FeCl_3$ treatment (Figure 3). Further, FeCl-Alg had a greater slope on the model than Ca-Alg ($K_1 = 9.1 \times 10^{-3}$ vs. 8.3×10^{-3}), indicating that FeCl-Alg approached adsorption equilibrium slightly faster (Table 1). The primary rate limiting factor for Ca-Alg was found to be surface diffusion rather than diffusion within the hydrogel according to the intraparticle diffusion model (C > 0, K_{id} = 15.2), while a poor fit for FeCl-Alg (R^2 = 0.79) indicated that multiple different steps and processes beyond diffusion controlled the rate, such as chemisorption (Table 1). However, despite being a poor fit for FeCl-Alg, its abnormally high boundary layer effect (C = 174.4) suggested a greater contribution of interactions on the hydrogel surface during the initial stages of adsorption.

Adsorption Capacity Analysis

Concentration (mg/L)	Ca-Alg (mg/g)	FeCl-Alg (mg/g)	p-value	Cohen's effect size
2	5.93±1.90	11.75±4.98	p = 0.012	d = 1.10
4	25.45±2.39	33.00±9.91	p = 0.017	d = 1.02
8	68.80±6.08	83.47±9.27	p = 0.001	d = 1.65
16	147.09±22.25	182.89±24.58	p = 0.005	d = 1.28
32	321.79±25.83	376.14±33.60	p = 0.001	d = 1.56

(a)

Time (min)	Ca-Alg (mg/g)	FeCl-Alg (mg/g)	p-value	Cohen's effect size
5	22.41±5.46	150.96±24.85	p < 0.001	d = 2.54
15	53.47±16.41	192.37±29.64	p = 0.017	d = 1.54
30	84.53±22.14	257.08±32.47	p < 0.001	d = 1.27
60	153.55±22.55	289.87±35.85	p < 0.001	d = 1.13
180	238.10±34.00	343.36±36.14	p < 0.001	d = 1.34
480	317.47±38.71	361.47±31.98	p = 0.031	d = 0.89

(b)

Table 2. A: The table shows the mean + standard deviation of the adsorption capacities of both hydrogel groups at initial phosphate concentrations 2-32 mg/L. n=10. B: The table shows the mean + standard deviation of the adsorption capacities of both hydrogel groups at different time intervals 5-480 min. The control group and the $FeCl_3$ modified hydrogels were immersed in varying concentrations of phosphate and recorded at different time intervals. T-tests were used to calculate significance ($p<0.05$) and effect size ($d>0.8$). n=10.

FeCl-Alg showed a statistically significant ($p < 0.05$) and meaningful ($d > 0.8$) improvement in adsorption capacity over Ca-Alg at all concentrations and time intervals, indicating the enhanced adsorption capabilities of FeCl-Alg (Table 2). This improved adsorption performance was also indicated by a higher Freundlich isotherm constant for FeCl-Alg compared to Ca-Alg (K_F = 0.578 mg/g vs. 0.332 mg/g, Table 1). Interestingly, FeCl-Alg demonstrated the highest adsorption capacity improvements in low concentrations and time intervals. One possible explanation is that the additional Fe(III) adsorption sites introduced through $FeCl_3$ treatment are readily available for phosphate binding during the initial stages of adsorption, resulting in faster initial uptake and adsorption efficiency before the available adsorption sites become saturated. This interpretation is consistent with previous studies reporting that increasing accessible iron adsorption sites improves phosphate removal efficiency (5, 6, 10, 11).

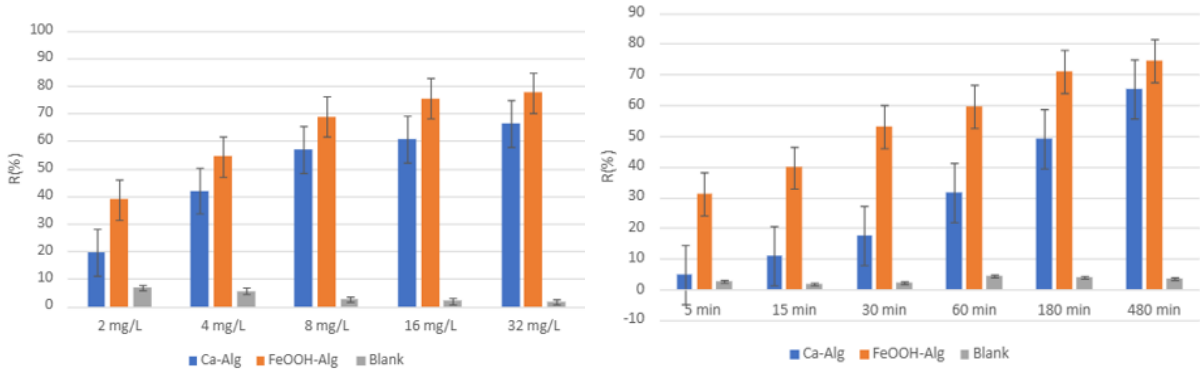
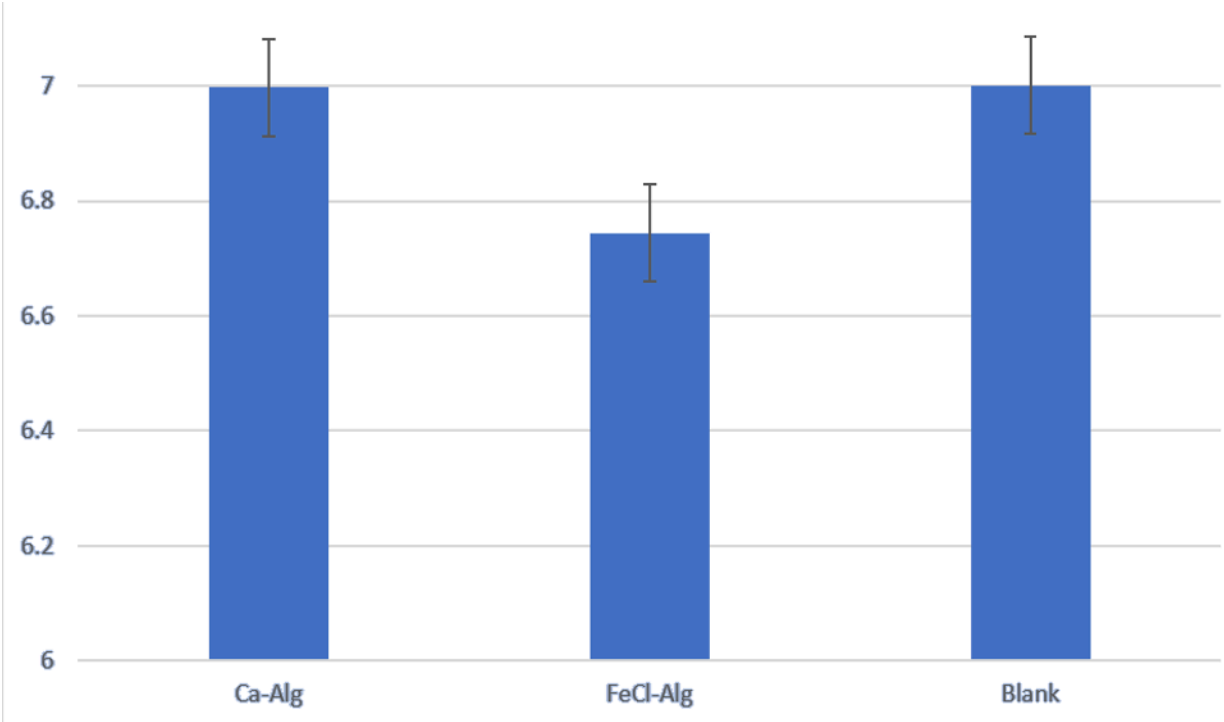


Figure 4. These bar graphs show the effects of different concentrations (C_o) and time intervals on the removal efficiency (R(%)) of varying hydrogel groups (Ca-Alg, FeCl-Alg) and a control group (Blank). R(%) was calculated by the removal efficiency equation, with C_o and time plotted against R(%). n=10.

FeCl-Alg consistently had a much greater percent adsorbate removal efficiency compared with Ca-Alg across time intervals and concentrations (Figure 4). Data from the blank groups also show that the calibration curve and colorimetric method were relatively reliable in their results, accurately determining stock concentrations.

pH Leaching Test



pH Values of Water After Immersed in Hydrogels.

Figure 5. This bar graph shows the mean pH values of different hydrogel groups to assess impact in aqueous conditions. Hydrogel groups (Ca-Alg, FeCl-Alg) and a control group (blank) were immersed in a solution of water, then measured with a pH meter. n=10.

The Ca-Alg group had negligible pH change in the leaching test (pH = 6.997), while FeCl-Alg had slightly acidic pH values (pH = 6.744), which could indicate the minor release of residual Fe(III) ions from the crosslinking process (Figure 5). However, for common wastewater systems, such a pH change is negligible and is unlikely to significantly affect the usability of the adsorbent (15). Thus, $FeCl_3$ treatment on the FeOOH-immobilized hydrogels did not significantly alter the surrounding aqueous conditions. A nearly neutral pH for the blank groups (pH = 7.001) indicated the accuracy of the pH meter.

DISCUSSION

The results suggest that $FeCl_3$ treatment of FeOOH-immobilized alginate hydrogels is successful at improving adsorption capacity and speed through the addition of additional Fe(III) sites. Overall, these findings support the hypothesis that $FeCl_3$ crosslinking of FeOOH immobilized alginate hydrogels would result in improved phosphate adsorption capacity and kinetics. Weak conformity of FeCl-Alg to kinetic models compared with strong pseudo-first-order behavior of Ca-Alg suggests a more complex adsorption process following $FeCl_3$ treatment. Furthermore, the increased adsorption capacity of FeCl-Alg indicates that $FeCl_3$ treatment improved the availability and concentration of adsorption sites within the hydrogel. These results suggest that $FeCl_3$ treatment increased the number of accessible Fe(III)-based adsorption sites available for phosphate binding, thereby increasing the probability for adsorption processes to occur. This is supported by prior literature, as Fe(III) ions exhibit strong affinity to phosphate through surface complexation and precipitation reactions (4, 5, 6). Large adsorption improvements at low concentrations and times further indicate the improved accessibility and availability of adsorption sites following $FeCl_3$ treatment.

The improved performance of FeCl-Alg is consistent with previous studies demonstrating that increasing the availability of iron-based adsorption sites enhances phosphate removal efficiency (5, 6, 10, 11). Previous FeOOH-based hydrogel systems have demonstrated the importance of available iron hydroxide binding sites for phosphate uptake, supporting the potential role of additional Fe(III)-based adsorption sites in the present study (10, 11). Success in the $FeCl_3$ crosslinking method further indicates similar success and the potential to improve the adsorption performance of previous FeOOH-based adsorbents with polymer backbones through additional crosslinking, such as hydrogels (10, 11), clay (8), melamine sponge (9), and aluminum hydroxide composites (3). This approach towards improving the adsorption capabilities of FeOOH-hydrogel adsorbents for the removal of phosphates and other pollutants in water research and wastewater treatment indicates the need for further research into iron-based polymer adsorbents and modification methods. As noted by Kim et al. (5), Wilfert et al. (6), Yang et al. (11), and other studies, the accessibility and interaction of Fe(III) species are critical factors controlling the

effectiveness of polymer adsorbents. Along with being highly effective at binding with phosphate, FeCl-Alg has various other potential benefits that would improve wastewater treatment. Faster and higher adsorption removal efficiencies of FeCl-Alg compared to previous systems could reduce operational costs and scalability. This is especially relevant as most wastewater treatment plants use iron-based materials for phosphate and other pollutant removal (6, 7). Through simply immersing adsorbents, like Ca-Alg, in solutions of $FeCl_3$, currently used polymer adsorbents may be modified to improve adsorption performance on a larger scale.

Recommendations for Future Study

Although FeCl-Alg demonstrated improved phosphate removal performance, future optimization of $FeCl_3$ treatment conditions and characterization of the hydrogel system are needed to fully understand and optimize the adsorption interactions. Future studies should also evaluate the long-term stability, regeneration, and reusability of FeCl-Alg over multiple adsorption cycles to assess its practical applicability. Nonetheless, a sustainable and effective method for improving polymer-supported iron hydroxide adsorbents has been investigated in this study, providing potential applications for future wastewater treatment systems. Lower concentrations of phosphate in wastewater would globally bring significant environmental and health benefits, as well as allowing for recovery of the limited valuable resource of phosphate. However, it is important to note potential other effects from $FeCl_3$ treatment that may also influence the hydrogel. As Fe(III) forms stronger crosslinks with alginate than Ca(II), $FeCl_3$ crosslinking may alter the hydrogels network structure, porosity, and swelling behavior, which could improve phosphate adsorption and transport (14). Additionally, $FeCl_3$ treatment could influence the surface chemistry of the FeOOH or create dissolved amorphous iron hydroxides, which could also influence the adsorption process, consistent with the proposed mechanism (4, 5, 6). These effects could also occur simultaneously with the increase in adsorption sites and contribute to the improved adsorption observed in FeCl-Alg. Further characterization, including measurements for dissolved iron, SEM imaging, BET surface area analysis, XPS, FTIR, zeta potential analysis, and structural measurements of the hydrogel, would provide necessary understanding of the specific contributions of these mechanisms to the adsorption process.

CONCLUSION

In conclusion, to address the need to improve the adsorption capabilities of FeOOH immobilized alginate hydrogels reported in prior literature, a $FeCl_3$ crosslinking modification was investigated and found to improve adsorption performance. Data suggests that additionally crosslinking FeOOH-immobilized alginate hydrogel with $FeCl_3$ (FeCl-Alg) enhances phosphate adsorption compared to conventional Ca-Alg through increased Fe(III)-based phosphate adsorption sites. Improved adsorption capacity and speed were observed in $FeCl_3$-Alg, suggesting a more efficient adsorption process. Moreover, FeCl-Alg had larger maximum adsorption capacity and percent removal values compared to Ca-Alg. Thus, FeCl-Alg improved upon prior methods, presenting a faster, more efficient, and scalable modification method to improve FeOOH-loaded alginate hydrogels.

ACKNOWLEDGMENTS

I would like to thank Professor Xi Chu of the University of Montana, who thoroughly reviewed this paper and gave invaluable insights and suggestions for improvement.

REFERENCES

1. Dodds, Walter K., et al. "Eutrophication of U.S. Freshwaters: Analysis of Potential Economic Damages." *Environmental Science & Technology*, vol. 43, no. 1, 2008, pp. 12–19. https://doi.org/10.1021/es801217q. Accessed 6 June 2026.
2. Conley, Daniel J., et al. "Controlling Eutrophication: Nitrogen and Phosphorus." *Science*, vol. 323, no. 5917, 2009, pp. 1014–15. https://doi.org/10.1126/science.1167755. Accessed 6 June 2026.
3. Xu, R., et al. "Enhanced Phosphorus Locking by Novel Lanthanum/Aluminum-Hydroxide Composite: Implications for Eutrophication Control." *Environmental Science & Technology*, vol. 51, no. 6, 2017, pp. 3418–25. https://doi.org/10.1021/acs.est.6b05623. Accessed 6 June 2026.
4. Dzombak, David A., and François M. M. Morel. "Surface Complexation Modeling: Hydrous Ferric Oxide." *Wiley*, 1990. Accessed 6 June 2026.
5. Kim, J., et al. "Phosphate Adsorption on the Iron Oxyhydroxides Goethite (α-FeOOH), Akaganeite (β-FeOOH), and Lepidocrocite (γ-FeOOH)" *Energy & Environmental Science*, vol. 4, no. 10, 2011, p. 4298. https://doi.org/10.1039/C1EE02093E. Accessed 6 June 2026.
6. Wilfert, Peter, et al. "The Relevance of Phosphorus and Iron Chemistry to the Recovery of Phosphorus from Wastewater: A Review." *Environmental Science & Technology*, vol. 49, no. 16, 2015, pp. 9400–14. https://doi.org/10.1021/acs.est.5b00150. Accessed 6 June 2026.
7. United States Environmental Protection Agency. "Phosphorus Removal by Ferrous Iron and Lime." Jan. 1971. https://nepis.epa.gov/Exe/ZyPURL.cgi?Dockey=9100W94V.TXT. Accessed 6 June 2026.
8. Ozola, R., et al. "FeOOH-Modified Clay Sorbents for Arsenic Removal from Aqueous Solutions." *Environmental Technology & Innovation*, vol. 13, 2019, pp. 364–72. https://doi.org/10.1016/j.eti.2016.06.003. Accessed 6 June 2026.
9. Tao, R., et al. "Preparation of FeOOH Supported by Melamine Sponge and Its Application for Efficient Phosphate Removal." *Journal of Environmental Chemical Engineering*, vol. 10, no. 4, 2022, article 108064. https://doi.org/10.1016/j.jece.2022.108064. Accessed 6 June 2026.
10. Yao, Z., et al. "A Novel Approach for Continuous Uptake of Phosphate Using FeOOH Hydrogel Beads with Phosphorus Accumulation for Recovery." *Separation and Purification Technology*, vol. 386, 2025, article 136566. https://doi.org/10.1016/j.seppur.2025.136566. Accessed 6 June 2026.
11. Yang, X., et al. "Highly Dispersed Amorphous FeOOH in Hydrogel Beads for Efficient Removal of Low-Concentration Phosphate from Water." *Desalination*, vol. 616, 2025, article 119405. https://doi.org/10.1016/j.desal.2025.119405. Accessed 6 June 2026.
12. Doan, L., K. T. Tran, and K. G. Huynh. "Surface Modifications of Superparamagnetic Iron Oxide Nanoparticles with Chitosan, Polyethylene Glycol, Polyvinyl Alcohol, and Polyvinylpyrrolidone as Methylene Blue Adsorbent Beads." *Polymers*, vol. 16, no. 13, 2024, article 1839. https://doi.org/10.3390/polym16131839. Accessed 6 June 2026.

13. Pierre, Alain C. "Introduction to Sol-Gel Processing." *Springer*, 2020. https://doi.org/10.1007/978-3-030-38144-8. Accessed 6 June 2026.
14. Massana Roquero, D., et al. "Iron(III)-Cross-Linked Alginate Hydrogels: A Critical Review." *Materials Advances*, vol. 3, no. 4, 2022, pp. 1849–73. https://doi.org/10.1039/D1MA00959A. Accessed 6 June 2026.
15. Hassen. "Cytotoxicity of Ferric Chloride Used as an Adjuvant of Organic Acid Precipitation." *Archives de l'Institut Pasteur de Tunis*, vol. 69, nos. 1–2, 1992. pubmed.ncbi.nlm.nih.gov/1489244/. Accessed 6 June 2026.
16. Cornell, R. M., and U. Schwertmann. "The Iron Oxides," *Wiley*, 2003.
17. Foo, K. Y., and B. H. Hameed. "Insights into the Modeling of Adsorption Isotherm Systems." *Chemical Engineering Journal*, vol. 156, no. 1, 2010, pp. 2–10. https://doi.org/10.1016/j.cej.2009.09.013. Accessed 6 June 2026.
18. Nasir, M., et al. "Regenerable Chitosan-Embedded Magnetic Iron Oxide Beads for Nitrate Removal from Industrial Wastewater." *Environmental Science: Advances*, vol. 3, no. 4, 2024, pp. 572–84. https://doi.org/10.1039/D3VA00351E. Accessed 6 June 2026.
19. Wang, J., and X. Guo. "Adsorption Kinetic Models: Physical Meanings, Applications and Solving Methods." *Journal of Hazardous Materials*, vol. 390, 2020, article 122156. https://doi.org/10.1016/j.jhazmat.2020.122156. Accessed 6 June 2026.